Arf-like Protein 2 (ARL2) Controls Microtubule Neogenesis during Early Postnatal Photoreceptor Development

Cecilia D. Gerstner[1], Michelle Reed[1], Tiffanie M. Dahl[1], Guoxin Ying[1], Jeanne M. Frederick[1] and Wolfgang Baehr[1,2,3]

[1]Department of Ophthalmology, University of Utah Health Science Center, Salt Lake City, Utah 84132, USA; cecilia.gerstner@hsc.utah.edu; michelle.reed1.618@gmail.com; g.ying@utah.edu ; tiffanie.dahl@gmail.com ; jeanne.frederick@hsc.utah.edu; wbaehr@hsc.utah.edu.

[2]Department of Neurobiology & Anatomy, University of Utah, Salt Lake City, USA

[3]Department of Biology, University of Utah, Salt Lake City, USA

Correspondence: E-mail *wbaehr@hsc.utah.edu*

Abstract: Arf-like protein 2 (ARL2) is a ubiquitously expressed small GTPase with multiple functions. In cell culture, ARL2 participates with tubulin cofactor D (TBCD) in the neogenesis of tubulin αβ-heterodimers, the building blocks of microtubules. To evaluate this function in retina, we conditionally deleted ARL2 in mouse retina at two distinct stages, either during embryonic development ($^{ret}Arl2^{-/-}$) or after ciliogenesis specifically in rods ($^{rod}Arl2^{-/-}$). $^{ret}Arl2^{-/-}$ retina sections displayed distorted nuclear layers and a disrupted microtubule cytoskeleton (MTC) as early as postnatal day 6 (P6). Rod and cone outer segments (OS) did not form. By contrast, rod ARL2 knockouts were stable at postnatal day 35 and revealed normal ERG responses. Cytoplasmic dynein is reduced in $^{ret}Arl2^{-/-}$ inner segments (IS), suggesting that dynein may be unstable in the absence of a normal MTC. We investigated microtubular stability in the absence of either ARL2 ($^{ret}ARL2^{-/-}$) or DYNC1H1 ($^{ret}Dync1h1^{-/-}$), the dynein heavy chain, and found that both the $^{ret}Arl2^{-/-}$ and $^{ret}Dync1h1^{-/-}$ retinas exhibited reduced microtubules and nuclear layer distortion. The results suggest that ARL2 and dynein depend on each other to generate a functional MTC during early photoreceptor development.

Keywords: Arf-like protein 2 (ARL2); tubulin αβ-heterodimers; retina; rod photoreceptors; microtubule cytoskeleton (MTC); dynein heavy chain (DYNC1H1);

1. Introduction

Arf-like (ARL) proteins of the Ras superfamily are small GTPases, discovered in *Drosophila* more than 30 years ago (1). Soon thereafter, mammalian ARLs were cloned (2,3) and to date, >22 genes encoding ARL proteins have been identified in mammalian genomes (4). ARL2 and ARL3 are the best characterized among ARLs (reviewed in (5). ARL2 is expressed ubiquitously in yeast (6) and plants (7). Gene mutations of the ARL2 ortholog, CIN4, in yeast cause aberrant chromosome numbers and defects of nuclear migration (6). In *C. elegans,* the ARL2 ortholog, evl-20, regulates MTC dynamics (8). ARL2 is highly conserved throughout eukaryotic evolution (9) and was shown to interact with PDE6δ (10-13), rootletin (14), BART (Binder of ARL2 or ARL2BP) (15-18) and CEP164 (19).

 doi:10.20944/preprints202211.0362.v1

In human, ARL2(R15L) is associated with MRCS syndrome (microcornea, rod-cone dystrophy, cataract and staphyloma) (20).

Within the mammalian retina, ARL2 localizes in the photoreceptor IS, with enrichment in the basal body area/rootlet (21). ARL2 has a relatively weak affinity to nucleotides and presumably exchanges GDP with GTP without Guanine nucleotide Exchange Factor (GEF) assistance (22,23). GAPs for ARL2 include ELMOD1-3 (ELMO Domain Containing 1-3), but these GAPs are not ARL2-specific (14,24-26). In cell culture, ARL2 associates with centrosomes throughout the cell cycle, and may be involved in regulation of mitochondrial fusion (27). ELMOD2 and ARL2 localize to the photoreceptor rootlet associated with the centrosomal γ-tubulin ring complex (γ-TuRC) at the basal body (14) which is involved in microtubule nucleation. ELMOD2 deletion in cell lines causes delay of the recruitment of γ-TuRC and microtubule nucleation from centrosomes (26). ELMOD3 deletion in mice leads to progressive hearing loss and abnormalities in cochlear hair cell stereocilia (28,29).

ARL2 and Tubulin Folding Cofactor D (TBCD) are key regulators in the assembly of αβ-tubulin heterodimers (see Graphical Abstract), the building blocks of photoreceptor axonemes and the IS MTC (30-33). Assembly of αβ tubulin heterodimers requires the participation of tubulin chaperones TBCA-D and formation of a super-complex consisting of TBCC-E and ARL2-GTP (22,31,32,34). Overexpression of TBCD caused microtubule depolymerization that was inhibited by coexpression with ARL2 (31,35). Expression of ARL2 with a dominant activating mutation (ARL2-Q70L) caused failure of tubulin polymerization, with loss of microtubules and microtubule-based mitotic spindle, resulting in cell cycle arrest in M phase (33). A transgenic model expressing ARL2-Q70L under a rod-specific promoter exhibited reduced photoreceptor cell function and progressive rod degeneration in the third postnatal week (21).

In this communication, we show that embryonic deletion of ARL2 strongly affects the status of the photoreceptor MTC during early development and distortion of the outer and inner nuclear layers. Microtubule formation was impaired at postnatal days 6 and 10 consistent with an important role of ARL2 in heterodimeric α- and β-tubulin biosynthesis. Outer segments (OS) did not form and electroretinography (ERG) a- and b-wave amplitudes were diminished. Cytoplasmic dynein levels of the IS were reduced or absent, suggesting that dynein survival depends on microtubules.

 doi:10.20944/preprints202211.0362.v1

2. Materials and Methods

2.1. Mice

Egfp-*Cetn2* mice Stock No. 008234 - CB6-Tg(CAG-EGFP/CETN2)3-4Jgg/J) and Six3Cre transgenic mice (36) (Stock No: 019755) were acquired from The Jackson Laboratory. iCre75 transgenic mice were generated at the University of Utah (37).

2.2. Generation of retina- and rod-specific knockout mice

We acquired a cell line (UC-Davis KOMP repository, allele name Arl2tm1a(KOMP)Wtsi) with a gene trap flanked by loxP and FRT sites in intron 1 and a third loxP site in intron 3. Gene-trapped mice were generated at the University of Utah Transgenic Core Facility by blastocyst injection. Germline transmission of the $Arl2^{GT}$ allele was verified by PCR using primers upstream and downstream of the loxP site in intron 1. A floxed *Arl2* allele ($Arl2^{F/+}$) was generated following FRT-FLP recombination with Flp-recombinase. Mice carrying the $Arl2^{F}$ allele were mated with C57BL/6J mice to remove the *rd8* mutation inherent in KOMP mice (38). $Arl2^{F/F}$ mice were crossed with Six3Cre (36) or iCre75 transgenic mice (37) to generate retina-specific $Arl2^{F/+}$;Six3Cre ($^{ret}Arl2^{+/-}$) or rod-specific $Arl2^{F/+}$;iCre75 ($^{rod}Arl2^{+/-}$) heterozygous mice. Mice were then backcrossed to $Arl2^{F/F}$ to generate experimental animals. For identification of centrioles and connecting cilia, select mice were maintained on an Egfp-Cetn2 background.

2.3. Genotyping

Genomic DNA was extracted from fresh tissue by dissolving tail clips or whole retina from P8-12 day old mice in 150 µL tail lysis buffer at 50-60˚C for 1-2 hour. Digests were centrifuged at 15000 rpm for 5 minutes. Supernatant was added to an equal volume of isopropanol and centrifuged at 15000 rpm for 5 minutes. The DNA pellet was rehydrated in 75 µL H_2O. Genotyping was achieved by polymerase chain reaction with EconoTaq® DNA polymerase (Lucigen) using the following primers. WT mice, CSD-F (5′-TGTCCTTCACTGGTTCCAAGTACCC) and CSD-ttr (5′-GACAAACTCATCACCCTTATGAAGCT) (483 bp); Post-Flip mice, CSD-F and CSD-ttr (655 bp); Post-Flp&cre *Arl2* mice, CSD-F (5′-TGTCCTTCACTGGTTCCAAGTACCC) and CSD-R (5′-CTGCCCAGATAAATAAGAAGCCAAT) (741 bp); Floxed Arl2 mice, CSD-loxF (5′-GAGATGGCGCAACGCAATTAATG) and CSD-R (341 bp); Presence of Six3Cre and iCre75 transgenes: Six3CreFor (5′-TCGATGCAAGGAGTGATGAG) and Six3CreRev (5′-TTCGGCTATACGTAACAGGG) (550 bp). iCreFor (5′-GGATGCCACCTCTGATGAAG) and iCreRev (5′- CACACCATTCTTTCTGACCCG) (650 bp). An internal control was carried out with oIMR8744-fwd CAA ATG TTG CTT GTC TGG TG and oIMR8745-rev GTC AGT CGA GTG CAC AGT TT generating an amplicon of the mouse T cell receptor delta chain gene. Internal positive controls show presence of DNA in the negative PCR reaction (JAX protocol 22365: Standard PCR Assay - Tg(TcrAND)53Hed), Version 1.3).

 doi:10.20944/preprints202211.0362.v1

2.4. Western blot

Retinas were lysed in PHEM buffer (60mM PIPES, 25mM HEPES, 10mM EGTA, and 4mM MgSO4). 30 ug of protein (Lowry assay) were separated by a 16% Bis-Tris gel using low-MW buffer (50 mM MES (compound-2 *N*-morpholino)ethanesulfonic acid); 50 mM Tris, 1 mM EDTA, 0.1% SDS). After protein transfer to 0.45 μm nitrocellulose membrane (ThermoFisher), the membrane was blocked using 5% milk in Tween Tris-buffered saline (TTBS) for 1 hour and then incubated overnight at 4˚C in polyclonal Arl2 antibody (diluted 1:1000, gift from Richard Kahn, Emory University) in the same buffer..The membrane was washed (10 min X 3) and incubated 2 hours in LI-COR secondary antibodies (mouse IR680 1:10K and rabbit IR800 1:4K). Following washes in 1X TTBS the membrane was scanned using a LI-COR Odyssey imaging system.

2.5. Confocal immunohistochemistry

Eyes were harvested on days P6, 10 and 15. Eyes were enucleated, anterior segments were removed and eyecups immersion-fixed (4% paraformaldehyde in 0.1M phosphate buffer, pH 7.4) for 1 hour on ice. The eyecups were cryoprotected by submersion in 15% sucrose in 0.1M phosphate buffer (30 min), followed by submersion in 30% sucrose in 0.1M phosphate buffer until the tissue equilibrated by sinking..The OCT-embedded eyecups were frozen and later cut at 14 μm. Sections were warmed at 37˚C for 30 minutes and washed (10 min X 3) in 1X TBS (Tris-buffered saline). Primary antibodies, raised in rabbit and directed against the following proteins, were used to label sections overnight at 4˚C in 5% goat serum-0.1% TritonX-100 in TBS: anti-ARL2 (gifts of Nick Cowan, NYU and Richard Kahn, Emory); rhodopsin (Abclonal, 1:1000 dilution); DYNC1H1 (Proteintech 12345-1-AP, 1:250); anti-CTBP2 (RIBEYE, BD Biosciences 612044, 1:10000); anti-GC1 (GUCY2E), monoclonal antibody IS4 (Kris Palczewski (UC-Irvine). Visualization was achieved using either goat anti-rabbit or goat anti-mouse secondary antibodies tagged with Alexafluor 488, 555, or 647 (1:500) and incubated for 1 hour at room temperature.

Tubulin immunohistochemistry was performed on tissue fixed as described (above), with the addition of 'antigen retrieval' after sectioning. Briefly, slides with sections were warmed 30 minutes and washed (10 min X 2) in TBS followed by antigen retrieval for 5 minutes in 0.1% SDS in TBS at room temperature. Slides were then rinsed quickly (5 min) in TBS. The following antibodies were diluted in 5% goat serum in TBS and incubated overnight at 4˚C: rabbit anti-TUBA1A (Proteintech 14555-1-AP) 1:25, mouse anti-TUBB3 (Sigma T8578) 1:100; monoclonal mouse anti-polyglutamylated tubulin IgM (Sigma, T9822) 1:250; mouse anti-acetylated α-tubulin IgG2b (Sigma T7451) 1:500.

Basal body labelling required light fixation of 4% paraformaldehyde for 10 minutes only. Slides were incubated at 37˚C for 30 minutes, rehydrated in 1X TBS by washing (10 min X 3), blocked in 5% normal goat serum in 1X TBS and incubated either 1hr at RT or overnight at 4˚C. Primary antibodies were diluted in blocking buffer (5% serum in TBS) to cover wells and incubated 2hr RT or overnight at 4ºC. The following antibodies were used: CEP250/CNAP1 antibody (14498-1-AP, Proteintech; rabbit anti-CEP164 (EMD Millipore ABE 2621) 1:250 or anti-CEP164 (1:350, Sigma-Aldrich)..After washing slides in

 doi:10.20944/preprints202211.0362.v1

1X TBS (10 min X 3), secondary antibodies were diluted in blocking buffer, applied to sections and sections were incubated 1hr at room temperature in the dark.
Images were acquired using a Zeiss LSM 800 confocal microscope with 63X objective. Figure 7 was post-processed with Airyscan. All genotypes of a given age and antibody were imaged at a single z-plane using identical settings for laser intensity and master gain. Digital gain = 1 for all images. Pinhole size was set for 1AU on the red channel (39 µm for the 40X objective). Post-processing of non-saturated images consisted of equal adjustments to brightness/contrast of control and knockout images using Adobe Photoshop but without affecting the conclusions made. Red channel separation was obtained by isolating the R-channel in the "blender options" of Adobe Photoshop.

2.6. Electroretinography

Scotopic and photopic ERG measurements were performed using P15-P18 for Six3Cre experiments and P35 for the iCre75 experiments. Prior to ERG the mice were dark-adapted overnight and anesthetized with intraperitoneal injection of 1% ketamine/0.1% xylazine at 10 µl/g body weight. The mice were kept warm during ERG by using a temperature-controlled stage. Scotopic and photopic responses were recorded as described (39-41) using a UTAS BigShot Ganzfeld system (LKC Technologies, Gaithersburg, MD). Scotopic single-flash responses were recorded at stimulus intensities of -4.5 log cd s·m^{-2} [log candela seconds per square meter] to 2.4 log cd s·m^{-2}). Mice were light-adapted under a background light of 1.48 log cd s·m^{-2} for 5 minutes prior to measuring photopic responses. Photopic single-flash responses of control and knockout were recorded at stimulus intensities of -0.1 log cd s·m^{-2} to 1.9 log cd s·m^{-2}.

2.7. Statistical analysis

We performed an unbalanced two-factor ANOVA to compare experimental and control animals for their quantified A- and B-wave ERG measurements across multiple ages. Post-hoc multiple comparison was performed using Tukey's honestly significant difference criterion. Statistical significance was determined using an alpha value of $p < 0.05$. ERG statistics were computed using MATLAB's statistical toolbox "anovan" and "multcompare" functions.

2.8. Data Availability Statement

Data supporting the reported results are shown in Figures 1-7. Additional data from our lab concerning DYNC1H1 and CEP164 can be found in (40-42) and (39), respectively.

3. Results

3.1. Generation of the retina- (^{ret}Arl2$^{-/-}$) and rod-specific (^{rod}Arl2$^{-/-}$) ARL2 knockouts

Mouse ARL2 (184 residues) is a small GTPase featuring a G domain and small coiled-coil domains (**Figure 1A**) encoded by a ~6500 bp gene with 5 exons (**Figure 1B**). To enable conditional knockouts, we acquired a cell line in which a gene trap flanked by loxP and

Preprints (www.preprints.org) | NOT PEER-REVIEWED | Posted: 21 November 2022 doi:10.20944/preprints202211.0362.v1

FRT sites was placed in intron 1 and a third loxP site was placed in intron 3 (**Figure 1C**). A floxed *Arl2* allele (*Arl2*^{F}) (**Figure 1D**) is generated following FRT-FLP recombination with Flp-recombinase. Deletion of ARL2 in retina was achieved by mating with Six3Cre transgenic mice (36) expressing Cre recombinase at embryonic day 9 (E9) to yield *Arl2*$^{F/F}$;Six3Cre knockouts (abbreviated as ^{ret}*Arl2*$^{-/-}$) (**Figure 1E**), or by mating with iCre75 transgenic mice expressing Cre recombinase under the control of the rhodopsin promoter to yield rod knockouts (^{rod}*Arl2*$^{-/-}$). In iCre75 mice, Cre expression occurs during the second postnatal week when photoreceptors are postmitotic. Deletion of exons 2 and 3 truncates ARL2 at residue 20 after exon 1 as exon 4 is out-of-frame. Genotyping (**Figure 1F-H**) confirmed presence of loxP (F), presence of Six3Cre (G, band of 450 bp), and loss of exons 2 and 3 at P6 (H) in both knockouts (for details see Figure 1 legend and Methods). Western blots with P10 ^{ret}*Arl2*$^{-/-}$ and P15 ^{rod}*Arl2*$^{-/-}$ retina confirmed absence of ARL2 (**Figure 1I, J**).

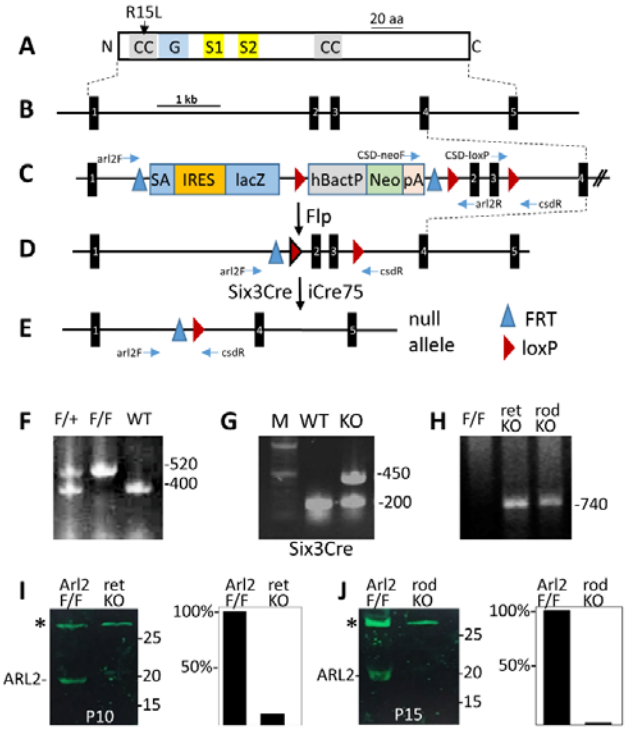

Figure 1. Generation of *Arl2* conditional knockouts. **A**, schematic of mouse ARL2 protein and its functional domains. CC, coiled coil domain; G, guanine nucleotide binding domain; S1 and S2, switch 1 and switch 2; R15L, mutation linked to retina disease. **B**, the mouse *Arl2* gene with 5 exons. **C**, the gene trap is located in intron 1. The gene trap is flanked by FRT sites. LoxP sites are flanking the NEO cassette and a third loxP site is placed in intron 3. Horizontal blue arrows delineate approximate positions of genotyping primers. **D**, floxed allele. **E**, null allele. **F**, genotyping floxed allele in tail DNA with arl2-F and arl2-R yielding a WT amplicon of 520 bp and a floxed amplicon of 400 bp. **G**, presence of Six3Cre in tail DNA using Six3Cre-F and Six3Cre-R yielding an amplicon of 450 bp. The bands of 200 bp are an internal positive control (see Methods). **H**, genotyping the Six3Cre (ret) and iCre65 (rod) knockout allele with CSDF and CSDR using retina DNA as a template.

 doi:10.20944/preprints202211.0362.v1

The diagnostic fragment of 740 bp is absent in Arl2 $^{F/F}$. **I, J**, western blots (left panels) with anti-ARL2 antibody using P10 ^{ret}*Arl2*$^{-/-}$ retina lysate (I) and P15 ^{rod}*Arl2*$^{-/-}$ retina lysate (J). Polypeptides marked with asterisks are nonspecific polypeptides serving as loading controls. I and J right panels are ImageJ density scans of ARL2.

3.2. ^{ret}*ARL2*$^{-/-}$ outer nuclear layers display abnormal histogenesis

We generated plastic sections at P10-P15 to study the phenotype of ^{ret}Arl2$^{-/-}$ retinas relative to controls. Control sections displayed normal photoreceptor IS and OS as well as correctly laminated nuclear layers (**Figure 2A-C**, left panels). By contrast, the nuclear layers, outer limiting membrane (OLM) and outer plexiform layers (OPL) of ^{ret}*Arl2*$^{-/-}$ retinas were severely distorted. ONL and INL thicknesses varied, the OPL was malformed with absence of outer segments, OLM interruptions and photoreceptor nuclear migration into the subretinal space nuclei (**Figure 2A-C**, right panels). We observed a similar photoreceptor phenotype of retina ONL/INL distortion in P6 ^{ret}*Dync1h1*$^{-/-}$ mice in which cytoplasmic dynein heavy chain 1 was deleted (41).

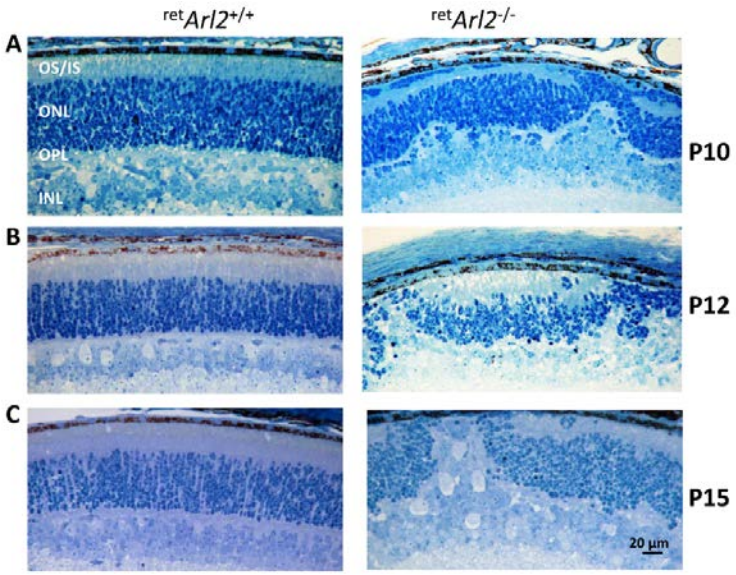

Figure 2. Histology of ^{ret}*Arl2*$^{-/-}$ sections at P10-15. **A-C,** plastic sections show histology of control (left panels) and ^{ret}Arl2$^{-/-}$ retinas (right panels) at days P10, P12 and P15. Note significant ONL/INL distortions, absence of OSs, abnormal ISs and displaced INL neurons in the P15 KO retina, reminiscent of retinas from *Dync1h1* knockouts.

3.3. Cytoplasmic dynein is unstable in ^{ret}*Arl2*$^{-/-}$ photoreceptors

Based on the ^{ret}*Arl2*$^{-/-}$ phenotype with ONL distortion (**Figure 2**), we suspected that cytoplasmic dynein, a multi-subunit complex organized around the heavy chain DYNC1H1, may be affected by the distorted/damaged MTC. Dynein transports cargo toward the minus-end of microtubules at the basal body and is essential for retina lamination, nuclear positioning, vesicular trafficking and inner/outer segment elaboration (41). Immunohistochemistry (IHC) of P6 and P10 control retina cryosections with anti-DYNC1H1 showed normal lamination of nuclear layers (**Figure 3A-D,**

Preprints (www.preprints.org) | NOT PEER-REVIEWED | Posted: 21 November 2022 doi:10.20944/preprints202211.0362.v1

left panels). A low magnification image of the entire P6 retina reveals presence of DYNC1H1 in IS, OPL and IPL of control retina (**Figure 3A**, left panel), but distorted ONL/INL layers and absence of DYNC1H1 (green) in IS and OPL of $^{ret}Arl2^{-/-}$ retina (**Figure 3A,** right panel). At P6, control OSs begin to form as guanylate cyclase 1 (GC1, gene nomenclature GUCY2E), a component of the phototransduction cascade, is detectable in budding OSs (**Figure 3B,** left panel. inset). GUCY2E is undetectable in $^{ret}Arl2^{-/-}$ sections (**Figure 3B**, right panel). In P6 controls, MTC labeled with anti-Ac-α-tubulin is well developed (**Figure 3C**, left panel), but severely distorted in the absence of ARL2 (**Figure 3C**, right panel). At P10, C-terminal binding protein 2 (CTBP2 alias RIBEYE) is located in the synaptic region of controls (**Figure 3D,** left panel). $^{ret}Arl2^{-/-}$ (**Figure 3D**, right panel) results reveal a thinning or absence of OPL, indicating defective synaptogenesis. Taken together, $^{ret}Arl2^{-/-}$ retina cryosections displayed distorted nuclear layers, reduction of DYNC1H1 in the IS and malformed microtubules.

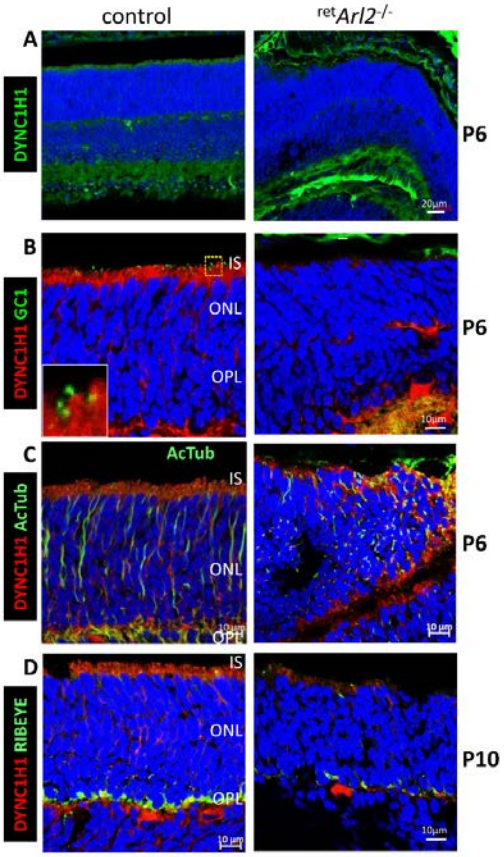

Figure 3. Immunohistochemistry with Arl2 cryosections. **A-D**, $^{ret}Arl2^{-/-}$ (right panels) and control cryosections (left panels) were probed with anti-DYNC1H1 (A-D), anti-GC1 (B), anti-PSD95 (C), and anti-RIBEYE (D) antibodies as indicated. A-C are postnatal day P6 cryosections, D is P10. Note distorted ONL, poorly developed OPL and suppression of DYNC1H1 fluorescence.

3.4.^{ret}Arl2$^{-/-}$ versus $^{rod}Arl2^{-/-}$ electroretinography

Functional analysis of $^{ret}Arl2^{-/-}$ retinas by pan-retina ERG at P15 and P18 demonstrated that average scotopic a- and photopic b-waves at 1.5 log cd s/m^2 were

Preprints (www.preprints.org) | NOT PEER-REVIEWED | Posted: 21 November 2022 doi:10.20944/preprints202211.0362.v1

severely diminished in the knockout (**Figure 4A, B**, red traces) consistent with absence of OS in the central retina. Average scotopic a- and photopic b-wave amplitudes as a function of light intensity (from -1.6 to 2.4 log cd s/m^2) were nearly extinguished (**Figure 4C, D**). Residual scotopic and photopic a- and b-waves are attributed to short photoreceptor OS formation, commonly observed with Six3Cre knockouts in the retina periphery where Six3Ce expression is delayed (41,43). By contrast, $^{rod}Arl2^{-/-}$ average ERG traces at P35 (N=5) and scotopic a- and photopic b-wave amplitudes as a function of light intensity (**Figure 4E-H**) indicate near-normal function of $^{rod}Arl2^{-/-}$ rods and cones. Scotopic a-waves and photopic b-waves were indistinguishable at intensities from -4.5 to 2.4 log cd s m^{-2}..We conclude that $^{rod}Arl2^{-/-}$ rod and cone OSs developed normally despite reduced αβ-tubulin heterodimer biosynthesis.

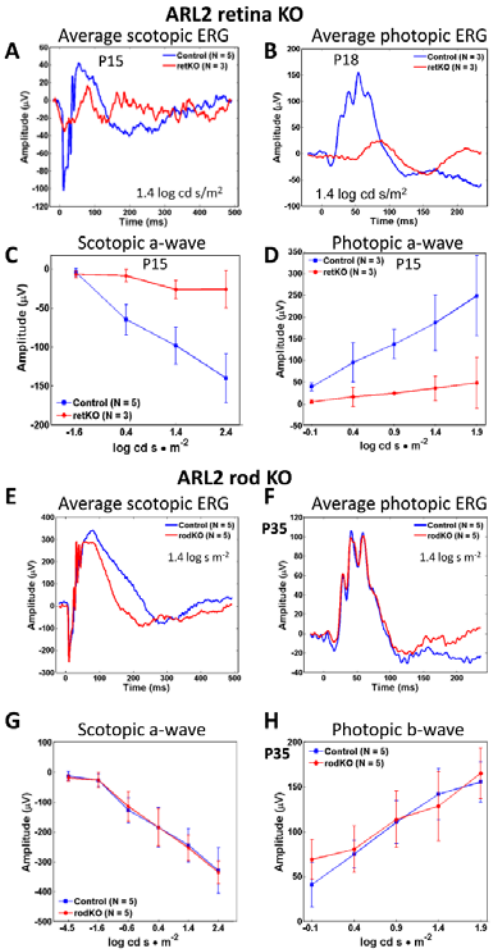

Figure 4. ERG of retina and rod ARL2 knockouts. **A, B**, averaged (n=3-5) pan-retina ERGs at P15 and P18. Average scotopic a- and photopic b-wave amplitudes revealed diminished amplitudes. Control ERGs are shown in blue, $^{ret}Arl2^{-/-}$ ERGs in red. **C, D**, scotopic a- and b-wave amplitudes as a function of light intensity. Note near complete extinction of responses. **E, F**, P35 rod knockout ERGs. Average scotopic a-wave (E) and photopic (F) b-wave amplitudes (n = 5) of control (blue) and rod KO (red) as a function of flash intensity. Control and knockout scotopic a- and b-wave amplitudes are nearly identical. **G, H**, scotopic a-wave (G) and photopic b-wave (H) as a function of light intensity. Rod knockouts shown in red, controls in blue.

Preprints (www.preprints.org) | NOT PEER-REVIEWED | Posted: 21 November 2022 doi:10.20944/preprints202211.0362.v1

3.5. Effect of ARL2 deletion on pericentriolar material

As ARL2 interacts with the basal body and the rootlet (14), we investigated effects of ARL2 deletion on the localization of basal body (BB) markers CEP164 and CEP250, employing EGFP-CETN2 to serve as a centriole and connecting cilium marker (39,41). CEP164 is a distal appendage protein surrounding the BB distal end (39,44,45) (**Figure 5A**) and is required for BB docking during photoreceptor development (14,46). BB docking and CC extension in $^{ret}Arl2^{-/-}$ photoreceptors is indistinguishable from controls (Fig 5A', B') but connecting cilia do not extend axonemes. Rather than being located at the inner segment cortex, $^{ret}Arl2^{-/-}$ BBs mislocalize within the $^{ret}Arl2^{-/-}$ ONL.

As ARL2 and rootletin are known interactants (14), we investigated whether ARL2 is involved in centriole cohesion. The centrosome linker proteins CEP250 (C-Nap1), rootletin (CROCC1), and CEP68 connect the mother and daughter centrioles during ciliogenesis (47,48). We probed P10 $Arl2^{F/F}$;Egfp-Cetn2^{+} (**Figure 5E**) and $^{ret}Arl2^{-/-}$;Egfp-Cetn2^{+} cryosections (**Figure 5F**) with anti-CEP250. The results show that C-NAP1 localizes between mother and daughter centrioles of both control and $^{ret}Arl2^{-/-}$ photoreceptors (**Figure 5C**) suggesting that ARL2 absence does not affect centriole cohesion.

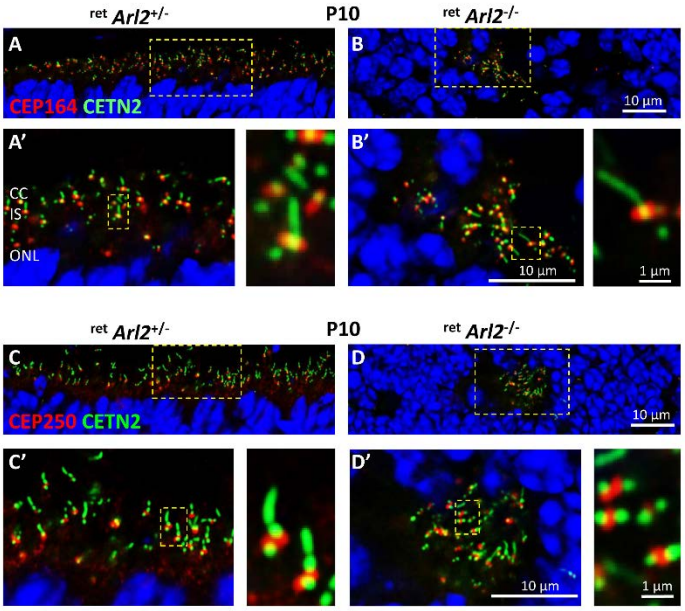

Figure 5. Basal body and CC are mislocalizing into the ONL. **A-F**, Immunohistochemistry of P10 control (A, A', C, C') and $^{ret}Arl2^{-/-}$ cryosections (B, B', D, D') probed with anti-CEP164 antibody (A, A', B, B'), and anti-CEP250 (C-NAP1) (C, C', D, D'). A'-D' are enlargements of A-D as indicted by yellow hatched boxes. To visualize individual rods, enlargement are shown next to A'-D'. In Arl2 knockout panels, the BB-CC structures are mislocalized into the ONL. CEP164 still enables docking of the basal body and extension of CC, and CEP250 still connects mother and daughter centrioles. Mice were kept on an EGFP-CETN2 transgenic background to mark centrioles and CC. Image was post-processed with Airy Scan of the LSM800 confocal microscope.

Preprints (www.preprints.org) | NOT PEER-REVIEWED | Posted: 21 November 2022 doi:10.20944/preprints202211.0362.v1

3.6. Microtubules are in disarray in the ARL2 knockout

The results shown in **Figure 3C** are consistent with an MTC defect, generated by absence of ARL2. The photoreceptor MTC is controlled by the microtubule organizing center (MTOC) consisting of the basal body and daughter centriole. The microtubule minus ends are anchored in the pericentriolar matrix and basal body (49). To test the status and stability of the $^{ret}Arl2^{-/-}$ MTC in the retina ONL and INL, we used anti-acetylated α-tubulin (Ac-Tub) and anti-polyglutamylated tubulin (polyE-Tub) antibodies to probe P6 and P10 retina cryosections (**Figure 6**). Acetylation of lysine 40 of α-tubulin and the addition of glutamate and glycine to both α- and β-tubulin, referred to as polyglutamylation and polyglycylation, are known to stabilize microtubules (reviewed in (50). Ac-Tub (white) and polyE-Tub (red) are labeled strongly at P6 and traverse the ONL of $Arl2^{F/F}$ retina (**Figure 6A, C**). At this age, Mueller glia which

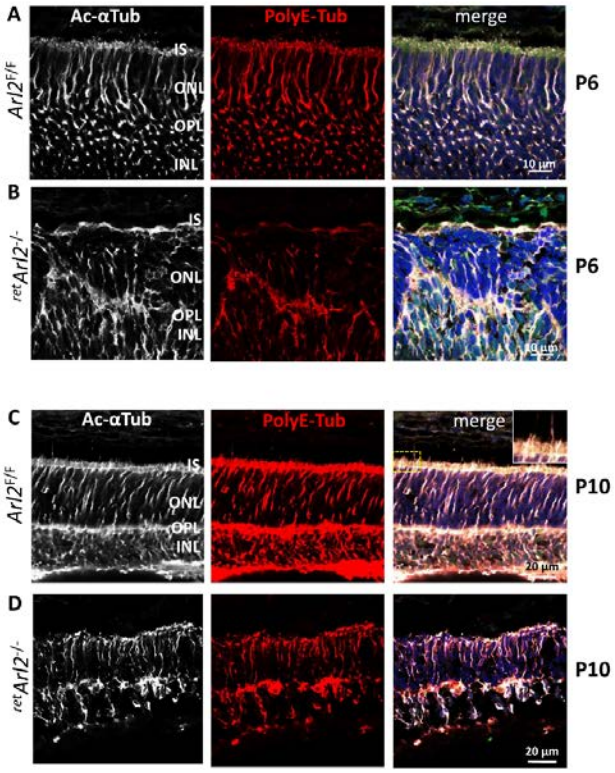

Figure 6. Immunohistochemistry of $^{ret}Arl2^{-/-}$ sections at P6 and P10. A-D, $^{ret}Arl2^{F/F}$ (rows A, C) and $^{ret}Arl2^{-/-}$ (rows B, D) retina cryosections probed with anti-acetylated α-tubulin (Ac-Tub, white, left column), anti-polyglutamylated tubulin (PolyE-Tub, red, middle column). The right column shows merged images of Ac-Tub and PolyE-Tub contrasted with DAPI to show the ONL. Note severe distortions of the ONL at P6 (row B) when ciliogenesis begins, but lesser distortions at P10 when OSs form (row D). A dashed rectangle in C (right panel) indicates the area of enlargements shown in row C (upper right corner).

penetrate the ONL at later ages are not detectable in the ONL/INL (41) (see discussion). At P10 photoreceptor OS are emerging, but labeling of the connecting cilia and axonemes by Ac-Tub and PolyE is relatively weak (**Figure 6C,** right panel, inset), in

Preprints (www.preprints.org) | NOT PEER-REVIEWED | Posted: 21 November 2022 doi:10.20944/preprints202211.0362.v1

contrast to a previous report where polyglutamylated microtubules are enriched at the photoreceptor connecting cilium (51). At P6 (**Figure 6B**), the $^{ret}Arl2^{-/-}$ ONL is strongly distorted, acetylated and polyglutamylated microtubules appear disrupted and significantly reduced. At P10, $^{ret}Arl2^{-/-}$ ONL appears to stabilize to a degree but ONL thickness is reduced, connecting cilia are not forming (Figure 4D') and photoreceptors are degenerating. Microtubules are severely reduced at P6 (**Figure 6B**) and P10 (**Figure 6D**) consistent with reduced levels of tubulin heterodimers in the absence of ARL2 (22,31,34). The results suggest that $^{ret}ARL2^{-/-}$ heterodimer output and MT formation is decreased, but not abolished.

3.7. Microtubule cytoskeleton is unstable in both $^{ret}ARL2^{-/-}$ and $^{ret}Dync1h1^{-/-}$ retina

The results suggest that absence of ARL2 early in postnatal development lowers tubulin heterodimer levels and affects MTC maturation which in turns affects dynein function. We investigated whether deletion of DYNC1H1, the key subunit of cytoplasmic dynein, would affect the MTC similarly as observed with ablation of ARL2. We compared the status of the P10 MTC in $^{ret}ARL2^{-/-}$ and P6 $^{ret}Dync1h1^{-/-}$ photoreceptors compared to controls by immunohistochemistry using anti-TUBA1A (α-1A tubulin, red) and anti-TUBB3 (β3-tubulin, green) antibodies (**Figure 7**). In control $Arl2^{F/F}$ and $Dync1h1^{F/F}$ sections, α- and β-tubulin form a normal photoreceptor cytoskeleton (**Figure 7A, C**). In $^{ret}Arl2^{-/-}$ (**Figure 7B**) and $^{ret}Dync1h1^{-/-}$ sections (**Figure 7D**), the MTC is disorganized and microtubules are severely reduced. The $^{ret}Dync1h1^{-/-}$ sections show reduced ONL thickness and near complete absence of microtubules (**Figure 7D**). This result indicates that dynein and ARL2 are essential for microtubule and MTC stabilization.

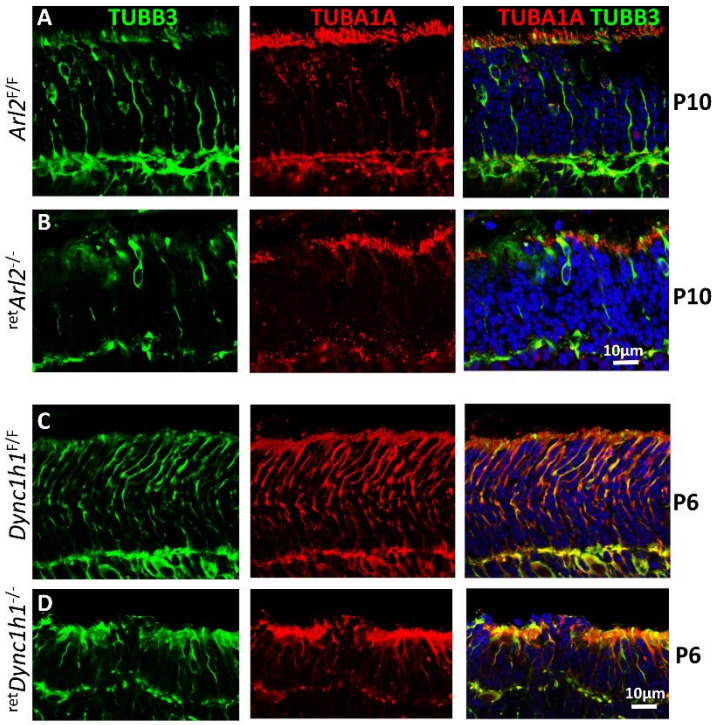

 doi:10.20944/preprints202211.0362.v1

Figure 7. Retina-specific deletion of Arl2 and DYNC1H1 damages the MTC. A-D, P10 *Arl2*$^{F/F}$ (row A), ^{ret}*Arl2*$^{-/-}$ (row B), P6 *Dync1H1*$^{F/F}$ (row C) and ^{ret}*Dync1h1*$^{-/-}$ cryosections (row D) probed with anti-TUBB3 (green) (A-D, left and right columns) and anti-TUBA1A antibodies (red) (middle and right columns). Note reduction of microtubules in knockout sections (B, D).

4. Discussion

To assess the status of the photoreceptor microtubules, we generated conditional retina and rod knockouts deleting ARL2 before and after ciliogenesis (**Figure 1**). Absence of ARL2 during early retina development affected the stability of ONL and INL (**Figure 2, 3**) and the MTC in photoreceptors as early as P6 (**Figure 6, 7**). OSs did not form in the central retina and ERG responses were diminished (**Figure 4**). ONL/INL distortion also affected the formation of the OPL and synapses (**Figure 3D**). The function of CEP164 (promoting docking of the basal body to the apical membrane and generating the connecting cilium) and CEP250 (required for centriole cohesion) were not affected, but connecting cilia did not localize to the cortex of the cell and were found misplaced within the ONL (**Figure 5**).

Apart from its function as release factor for prenylated proteins bound to PDE6D (52), ARL2 is involved in biosynthesis of αβ-tubulin heterodimers, the building blocks of microtubules (22,53,54). The history of ARL2 as a factor in tubulin heterodimer biosynthesis is well documented (30,34,55,56). Assembly of the αβ-tubulin dimer occurs in a folding cycle following biosynthesis of α- and β-tubulins, a highly controlled process (see graphical abstract). Assembly requires orchestrated action of a set of proteins of the chaperonin-containing TCP1 complex (CCT) (57), as well as tubulin-specific co-factors, i.e., TBCA-D (31,32,53). *In-vitro* biochemical studies revealed that α-tubulin binds to TBCB and β-tubulin to TBCA that are replaced by TBCD and TBCE (32,53). ARL2 when bound to TBCD exchanges GDP with GTP and plays a critical role in formation of a super complex consisting of TBCC/TBCE/α-tubulin and TBCD/β-tubulin/ARL2-GTP. Following release of TBCD and TBCE, triggered by GTP hydrolysis, α-tubulin and β-tubulin are released as heterodimers. The consequence is that, in the absence of ARL2, tubulin heterodimer levels are reduced thereby affecting microtubule assembly (see graphical abstract). Low levels of heterodimers during early photoreceptor development effectively curtail production of MT filaments which are necessary to stabilize dynein.

In *Drosophila melanogaster* neuroblasts, Arl2 physically associates with tubulin cofactors C, D, and E. Arl2 RNA interference, Arl2-GDP expression, or Arl2 deletions caused microtubule abnormalities suggesting that ARL2 regulates microtubule growth (58). *Chen, et al* conclude that Arl2 and cofactors are probably responsible for exquisitely regulating free tubulin heterodimer levels in the cell and localization of dynein at microtubules. However, knockdown of ARL2 by siRNA in tissue culture produced conflicting results. Deletion of ARL2 in immortal HeLa cells did not produce a phenotype (33), but silencing ARL2 in human neural progenitor cells provoked an apoptotic phenotype (59). Depletion of Arl2 by siRNA in human cell lines resulted in

 doi:10.20944/preprints202211.0362.v1

TBCD-mediated microtubule disruption (31). ARL2 siRNA significantly reduced the cilia lengths of ARPE19 cells (15).

We observed that cytoplasmic dynein levels in the photoreceptor IS were reduced in $^{ret}Arl2^{-/-}$ photoreceptors compared to controls (**Figure 3**) suggesting cytoplasmic dynein may become unstable in the absence of microtubule tracks. We previously observed that ablation of the dynein heavy chain in retina negatively affected MTC stability (41). We therefore tested whether microtubules and dynein are interdependent for stability. Floxed *Dync1h1* P6 retina cryosections probed with anti-TUBB3 and anti-TUBA1A revealed a stable MTC comparable to Arl2 controls (**Figure 7C**). By contrast, *Dync1h1*$^{-/-}$ sections revealed a severely attenuated ONL with an unstable MTC with few intact microtubules (**Figure 7D**). The effect on microtubules in $^{ret}Arl2^{-/-}$ sections is less dramatic, presumably because removal of ARL2 reduces but not obliterates tubulin heterodimer levels. MTC instability in the ONL could be in part caused by degenerating Mueller glia. However, at P6, Mueller glia processes are not detectable in the ONL/INL, and begin to penetrate the ONL after P10, as we have shown using anti-glutamine synthase as a marker (41) (Supplemental Figure 1). Therefore instability of the ONL MTC is most likely caused by reduced availability of tubulin heterodimers in photoreceptor axons. Direct interaction of ARL2 with cytoplasmic dynein has not previously been reported, to the best of our knowledge. A link between microtubule stability and dynein-2 (IFT dynein) has been provided in *Tetrahymena*. Microtubules of a microtubule-dynein-2 complex appear intact under conditions that result in microtubule depolymerization. When dynein was dissociated from the complex with addition of ATP, no microtubules were found in specimens under the same depolymerizing conditions suggesting microtubule catastrophe (60).

Surprisingly, the $^{rod}Arl2^{-/-}$ retina (rod knockout) is stable and functional in the first six postnatal weeks (**Figure 4E-H**). Tubulin heterodimer biosynthesis is expected to slowly decrease in $^{rod}Arl2^{-/-}$ mice in the first two postnatal weeks before Cre expression under the control of the rhodopsin promoter begins. An MTC can be established and photoreceptors mature. After onset of Cre expression, visible by immunohistochemistry around P16 (Dahl et al, 2021), ARL2 is knocked out but tubulin heterodimer apparently is still produced at levels sufficient to maintain the MTC. These findings suggest that the effect of ARL2 inactivation are defined by a developmental switch ending the rod maturation phase (P6-P16). In the early developmental phase, photoreceptors are building the MTC requiring high levels of tubulin, establish nuclear layers and IS and OS. In the mature phase (>P16), rods are more stable and can tolerate loss of ARL2 and reductions in heterodimers. An example for a developmental switch is the PKD1 (polycystin-1) knockout. In a mouse *Pkd1* conditional knockout model, inactivation of PKD1 before postnatal day 13 results in the formation of severe cystic kidney cysts within 3 weeks, whereas inactivation at day 14 and later results in cysts only after 5 months. These findings suggest that the effects of *Pkd1* inactivation are defined by a developmental switch that signals the end of the terminal renal maturation process (61).

 doi:10.20944/preprints202211.0362.v1

5. Conclusion

ARL2 is a multifunctional protein expressed in vertebrates, invertebrates, yeast and plants. Our results suggest that during early photoreceptor development, the photoreceptor microtubule cytoskeleton is unstable due to insufficient production of tubulin heterodimers. We suggest that the $^{ret}Arl2^{-/-}$ phenotype appears to be a consequence of a triple insult—impaired tubulin heterodimer synthesis, reduced microtubule assembly giving rise to a nonfunctional MTC, and downregulation of dynein. By contrast the $^{rod}Arl2^{-/-}$ photoreceptors are stable and can tolerate loss of ARL2 and reductions in heterodimers.

Author contributions: Conceptualization, WB and CDG; Methodology, CDG, MR, TMD and JMF; Data curation and formal analysis, CDG, MR, GY, JMF, and WB; Writing – Original Draft Preparation, WB; Writing – Review & Editing, CDG, MR, TMD, JMF, and GY; Funding acquisition, WB.

Funding: This work was supported by NIH grants EY08123, EY019298 (WB); EY014800-039003 (NEI core grant), 5T32 EY024234 (NEI training grant), by unrestricted grants to the University of Utah Department of Ophthalmology from Research to Prevent Blindness (RPB; New York) and by a grant from the Retina Research Foundation-Houston (Alice McPherson, MD).

Institutional Review Board Statement: The study was conducted according to guidelines of the Declaration of Helsinki, and approved by the University of Utah Institutional Animal Care and Use Committee (Protocol 18-11005).

Acknowledgments. We thank Richard Kahn (Emory) for anti-ARL2 antibodies,

Conflicts of Interest: The authors declare no conflict of interest.

 doi:10.20944/preprints202211.0362.v1

References

1. Tamkun, J. W., Kahn, R. A., Kissinger, M., Brizuela, B. J., Rulka, C., Scott, M. P., and Kennison, J. A. (1991) The arflike gene encodes an essential GTP-binding protein in Drosophila. *Proc. Natl. Acad. Sci. U. S. A* **88**, 3120-3124
2. Cavenagh, M. M., Breiner, M., Schurmann, A., Rosenwald, A. G., Terui, T., Zhang, C., Randazzo, P. A., Adams, M., Joost, H. G., and Kahn, R. A. (1994) ADP-ribosylation factor (ARF)-like 3, a new member of the ARF family of GTP-binding proteins cloned from human and rat tissues. *J Biol. Chem* **269**, 18937-18942
3. Schurmann, A., Breiner, M., Becker, W., Huppertz, C., Kainulainen, H., Kentrup, H., and Joost, H. G. (1994) Cloning of two novel ADP-ribosylation factor-like proteins and characterization of their differential expression in 3T3-L1 cells. *J Biol Chem* **269**, 15683-15688
4. Sztul, E., Chen, P. W., Casanova, J. E., Cherfils, J., Dacks, J. B., Lambright, D. G., Lee, F. S., Randazzo, P. A., Santy, L. C., Schurmann, A., Wilhelmi, I., Yohe, M. E., and Kahn, R. A. (2019) ARF GTPases and their GEFs and GAPs: concepts and challenges. *Mol Biol Cell* **30**, 1249-1271
5. Fisher, S., Kuna, D., Caspary, T., Kahn, R. A., and Sztul, E. (2020) ARF family GTPases with links to cilia. *Am J Physiol Cell Physiol* **319**, C404-C418
6. Hoyt, M. A., Stearns, T., and Botstein, D. (1990) Chromosome instability mutants of Saccharomyces cerevisiae that are defective in microtubule-mediated processes. *Mol Cell Biol* **10**, 223-234
7. McElver, J., Patton, D., Rumbaugh, M., Liu, C., Yang, L. J., and Meinke, D. (2000) The TITAN5 gene of Arabidopsis encodes a protein related to the ADP ribosylation factor family of GTP binding proteins. *Plant Cell* **12**, 1379-1392
8. Antoshechkin, I., and Han, M. (2002) The C. elegans evl-20 gene is a homolog of the small GTPase ARL2 and regulates cytoskeleton dynamics during cytokinesis and morphogenesis. *Dev. Cell* **2**, 579-591
9. Li, Y., Kelly, W. G., Logsdon, J. M., Jr., Schurko, A. M., Harfe, B. D., Hill-Harfe, K. L., and Kahn, R. A. (2004) Functional genomic analysis of the ADP-ribosylation factor family of GTPases: phylogeny among diverse eukaryotes and function in C. elegans. *FASEB J* **18**, 1834-1850
10. Hanzal-Bayer, M., Renault, L., Roversi, P., Wittinghofer, A., and Hillig, R. C. (2002) The complex of Arl2-GTP and PDE delta: from structure to function. *EMBO J* **21**, 2095-2106
11. Bos, J. L., Rehmann, H., and Wittinghofer, A. (2007) GEFs and GAPs: critical elements in the control of small G proteins. *Cell* **129**, 865-877
12. Ismail, S. A., Chen, Y. X., Miertzschke, M., Vetter, I. R., Koerner, C., and Wittinghofer, A. (2012) Structural basis for Arl3-specific release of myristoylated ciliary cargo from UNC119. *EMBO J* **31**, 4085-4094
13. Watzlich, D., Vetter, I., Gotthardt, K., Miertzschke, M., Chen, Y. X., Wittinghofer, A., and Ismail, S. (2013) The interplay between RPGR, PDEdelta and Arl2/3 regulate the ciliary targeting of farnesylated cargo. *EMBO Rep* **14**, 465-472
14. Turn, R. E., Linnert, J., Gigante, E. D., Wolfrum, U., Caspary, T., and Kahn, R. A. (2021) "Roles for ELMOD2 and Rootletin in Ciliogenesis". *Mol Biol Cell*, mbcE20100635
15. Davidson, A. E., Schwarz, N., Zelinger, L., Stern-Schneider, G., Shoemark, A., Spitzbarth, B., Gross, M., Laxer, U., Sosna, J., Sergouniotis, P. I., Waseem, N. H., Wilson, R., Kahn, R. A., Plagnol, V., Wolfrum, U., Banin, E., Hardcastle, A. J., Cheetham, M. E., Sharon, D., and Webster, A. R. (2013) Mutations in ARL2BP, encoding ADP-ribosylation-factor-like 2 binding protein, cause autosomal-recessive retinitis pigmentosa. *Am. J. Hum. Genet* **93**, 321-329
16. Moye, A. R., Bedoni, N., Cunningham, J. G., Sanzhaeva, U., Tucker, E. S., Mathers, P., Peter, V. G., Quinodoz, M., Paris, L. P., Coutinho-Santos, L., Camacho, P., Purcell, M. G., Winkelmann, A. C., Foster, J. A., Pugacheva, E. N., Rivolta, C., and Ramamurthy, V. (2019) Mutations in ARL2BP, a protein required for ciliary microtubule structure, cause syndromic male infertility in humans and mice. *PLoS Genet* **15**, e1008315

17. Moye, A. R., Singh, R., Kimler, V. A., Dilan, T. L., Munezero, D., Saravanan, T., Goldberg, A. F. X., and Ramamurthy, V. (2018) ARL2BP, a protein linked to retinitis pigmentosa, is needed for normal photoreceptor cilia doublets and outer segment structure. *Mol Biol Cell* **29**, 1590-1598
18. Sharer, J. D., and Kahn, R. A. (1999) The ARF-like 2 (ARL2)-binding protein, BART. Purification, cloning, and initial characterization. *J. Biol. Chem* **274**, 27553-27561
19. Humbert, M. C., Weihbrecht, K., Searby, C. C., Li, Y., Pope, R. M., Sheffield, V. C., and Seo, S. (2012) ARL13B, PDE6D, and CEP164 form a functional network for INPP5E ciliary targeting. *Proc. Natl. Acad. Sci. U. S. A* **109**, 19691-19696
20. Cai, X. B., Wu, K. C., Zhang, X., Lv, J. N., Jin, G. H., Xiang, L., Chen, J., Huang, X. F., Pan, D., Lu, B., Lu, F., Qu, J., and Jin, Z. B. (2019) Whole-exome sequencing identified ARL2 as a novel candidate gene for MRCS (microcornea, rod-cone dystrophy, cataract, and posterior staphyloma) syndrome. *Clin Genet* **96**, 61-71
21. Wright, Z. C., Loskutov, Y., Murphy, D., Stoilov, P., Pugacheva, E., Goldberg, A. F. X., and Ramamurthy, V. (2018) ADP-Ribosylation Factor-Like 2 (ARL2) regulates cilia stability and development of outer segments in rod photoreceptor neurons. *Sci Rep* **8**, 16967
22. Francis, J. W., Goswami, D., Novick, S. J., Pascal, B. D., Weikum, E. R., Ortlund, E. A., Griffin, P. R., and Kahn, R. A. (2017) Nucleotide Binding to ARL2 in the TBCDARL2beta-Tubulin Complex Drives Conformational Changes in beta-Tubulin. *J Mol Biol* **429**, 3696-3716
23. Fansa, E. K., and Wittinghofer, A. (2016) Sorting of lipidated cargo by the Arl2/Arl3 system. *Small GTPases* **7**, 222-230
24. Schiavon, C. R., Turn, R. E., Newman, L. E., and Kahn, R. A. (2019) ELMOD2 regulates mitochondrial fusion in a mitofusin-dependent manner, downstream of ARL2. *Mol Biol Cell* **30**, 1198-1213
25. Bowzard, J. B., Cheng, D., Peng, J., and Kahn, R. A. (2007) ELMOD2 is an Arl2 GTPase-activating protein that also acts on Arfs. *J. Biol. Chem* **282**, 17568-17580
26. Turn, R. E., East, M. P., Prekeris, R., and Kahn, R. A. (2020) The ARF GAP ELMOD2 acts with different GTPases to regulate centrosomal microtubule nucleation and cytokinesis. *Mol Biol Cell* **31**, 2070-2091
27. Newman, L. E., Schiavon, C. R., Turn, R. E., and Kahn, R. A. (2017) The ARL2 GTPase regulates mitochondrial fusion from the intermembrane space. *Cell Logist* **7**, e1340104
28. Li, W., Feng, Y., Chen, A., Li, T., Huang, S., Liu, J., Liu, X., Liu, Y., Gao, J., Yan, D., Sun, J., Mei, L., Liu, X., and Ling, J. (2019) Elmod3 knockout leads to progressive hearing loss and abnormalities in cochlear hair cell stereocilia. *Hum Mol Genet* **28**, 4103-4112
29. Ivanova, A. A., East, M. P., Yi, S. L., and Kahn, R. A. (2014) Characterization of recombinant ELMOD (cell engulfment and motility domain) proteins as GTPase-activating proteins (GAPs) for ARF family GTPases. *J Biol Chem* **289**, 11111-11121
30. Tian, G., and Cowan, N. J. (2013) Tubulin-specific chaperones: components of a molecular machine that assembles the alpha/beta heterodimer. *Methods Cell Biol* **115**, 155-171
31. Tian, G., Thomas, S., and Cowan, N. J. (2010) Effect of TBCD and its regulatory interactor Arl2 on tubulin and microtubule integrity. *Cytoskeleton (Hoboken)* **67**, 706-714
32. Tian, G., Huang, Y., Rommelaere, H., Vandekerckhove, J., Ampe, C., and Cowan, N. J. (1996) Pathway leading to correctly folded beta-tubulin. *Cell* **86**, 287-296
33. Zhou, C., Cunningham, L., Marcus, A. I., Li, Y., and Kahn, R. A. (2006) Arl2 and Arl3 regulate different microtubule-dependent processes. *Mol Biol Cell* **17**, 2476-2487
34. Francis, J. W., Newman, L. E., Cunningham, L. A., and Kahn, R. A. (2017) A Trimer Consisting of the Tubulin-specific Chaperone D (TBCD), Regulatory GTPase ARL2, and beta-Tubulin Is Required for Maintaining the Microtubule Network. *J Biol Chem* **292**, 4336-4349

35. Bhamidipati, A., Lewis, S. A., and Cowan, N. J. (2000) ADP ribosylation factor-like protein 2 (Arl2) regulates the interaction of tubulin-folding cofactor D with native tubulin. *J Cell Biol* **149**, 1087-1096
36. Furuta, Y., Lagutin, O., Hogan, B. L., and Oliver, G. C. (2000) Retina- and ventral forebrain-specific Cre recombinase activity in transgenic mice. *Genesis* **26**, 130-132
37. Li, S., Chen, D., Sauve, Y., McCandless, J., Chen, Y. J., and Chen, C. K. (2005) Rhodopsin-iCre transgenic mouse line for Cre-mediated rod-specific gene targeting. *Genesis* **41**, 73-80
38. Mattapallil, M. J., Wawrousek, E. F., Chan, C. C., Zhao, H., Roychoudhury, J., Ferguson, T. A., and Caspi, R. R. (2012) The Rd8 mutation of the Crb1 gene is present in vendor lines of C57BL/6N mice and embryonic stem cells, and confounds ocular induced mutant phenotypes. *Invest. Ophthalmol. Vis. Sci* **53**, 2921-2927
39. Reed, M., Takemaru, K. I., Ying, G., Frederick, J. M., and Baehr, W. (2022) Deletion of CEP164 in mouse photoreceptors post-ciliogenesis interrupts ciliary intraflagellar transport (IFT). *PLoS Genet* **18**, e1010154
40. Dahl, T. M., Reed, M., Gerstner, C. D., and Baehr, W. (2021) Conditional Deletion of Cytoplasmic Dynein Heavy Chain in Postnatal Photoreceptors. *Invest Ophthalmol Vis Sci* **62**, 23
41. Dahl, T. M., Reed, M., Gerstner, C. D., Ying, G., and Baehr, W. (2021) Effect of conditional deletion of cytoplasmic dynein heavy chain DYNC1H1 on postnatal photoreceptors. *PLoS One* **16**, e0248354
42. Dahl, T. M., and Baehr, W. (2021) Review: Cytoplasmic dynein motors in photoreceptors. *Mol Vis* **27**, 506-517
43. Sharif, A. S., Gerstner, C. D., Cady, M. A., Arshavsky, V. Y., Mitchell, C., Ying, G., Frederick, J. M., and Baehr, W. (2021) Deletion of the phosphatase INPP5E in the murine retina impairs photoreceptor axoneme formation and prevents disc morphogenesis. *J Biol Chem* **296**, 100529
44. Lau, L., Lee, Y. L., Sahl, S. J., Stearns, T., and Moerner, W. E. (2012) STED microscopy with optimized labeling density reveals 9-fold arrangement of a centriole protein. *Biophys J* **102**, 2926-2935
45. Yang, T. T., Chong, W. M., Wang, W. J., Mazo, G., Tanos, B., Chen, Z., Tran, T. M. N., Chen, Y. D., Weng, R. R., Huang, C. E., Jane, W. N., Tsou, M. B., and Liao, J. C. (2018) Super-resolution architecture of mammalian centriole distal appendages reveals distinct blade and matrix functional components. *Nat Commun* **9**, 2023
46. Spektor, A., Tsang, W. Y., Khoo, D., and Dynlacht, B. D. (2007) Cep97 and CP110 suppress a cilia assembly program. *Cell* **130**, 678-690
47. Vlijm, R., Li, X., Panic, M., Ruthnick, D., Hata, S., Herrmannsdorfer, F., Kuner, T., Heilemann, M., Engelhardt, J., Hell, S. W., and Schiebel, E. (2018) STED nanoscopy of the centrosome linker reveals a CEP68-organized, periodic rootletin network anchored to a C-Nap1 ring at centrioles. *Proc Natl Acad Sci U S A* **115**, E2246-E2253
48. Yang, J., and Li, T. (2006) Focus on molecules: rootletin. *Exp Eye Res* **83**, 1-2
49. Baehr, W., Hanke-Gogokhia, C., Sharif, A., Reed, M., Dahl, T., Frederick, J. M., and Ying, G. (2019) Insights into photoreceptor ciliogenesis revealed by animal models. *Prog Retin Eye Res* **71**, 26-56
50. Janke, C., and Magiera, M. M. (2020) The tubulin code and its role in controlling microtubule properties and functions. *Nat Rev Mol Cell Biol* **21**, 307-326
51. Bosch Grau, M., Masson, C., Gadadhar, S., Rocha, C., Tort, O., Marques Sousa, P., Vacher, S., Bieche, I., and Janke, C. (2017) Alterations in the balance of tubulin glycylation and glutamylation in photoreceptors leads to retinal degeneration. *J Cell Sci* **130**, 938-949
52. Ismail, S. A., Chen, Y. X., Rusinova, A., Chandra, A., Bierbaum, M., Gremer, L., Triola, G., Waldmann, H., Bastiaens, P. I., and Wittinghofer, A. (2011) Arl2-GTP and Arl3-GTP regulate a GDI-like transport system for farnesylated cargo. *Nat Chem Biol* **7**, 942-949
53. Lewis, S. A., Tian, G., and Cowan, N. J. (1997) The alpha- and beta-tubulin folding pathways. *Trends Cell Biol* **7**, 479-484

54. Nithianantham, S., Le, S., Seto, E., Jia, W., Leary, J., Corbett, K. D., Moore, J. K., and Al-Bassam, J. (2015) Tubulin cofactors and Arl2 are cage-like chaperones that regulate the soluble alphabeta-tubulin pool for microtubule dynamics. *Elife* **4**
55. Bowzard, J. B., Sharer, J. D., and Kahn, R. A. (2005) Assays used in the analysis of Arl2 and its binding partners. *Methods Enzymol* **404**, 453-467
56. Cunningham, L. A., and Kahn, R. A. (2008) Cofactor D functions as a centrosomal protein and is required for the recruitment of the gamma-tubulin ring complex at centrosomes and organization of the mitotic spindle. *J Biol Chem* **283**, 7155-7165
57. Yaffe, M. B., Farr, G. W., Miklos, D., Horwich, A. L., Sternlicht, M. L., and Sternlicht, H. (1992) TCP1 complex is a molecular chaperone in tubulin biogenesis. *Nature* **358**, 245-248
58. Chen, K., Koe, C. T., Xing, Z. B., Tian, X., Rossi, F., Wang, C., Tang, Q., Zong, W., Hong, W. J., Taneja, R., Yu, F., Gonzalez, C., Wu, C., Endow, S., and Wang, H. (2016) Arl2- and Msps-dependent microtubule growth governs asymmetric division. *J Cell Biol* **212**, 661-676
59. Zhou, Y., Jiang, H., Gu, J., Tang, Y., Shen, N., and Jin, Y. (2013) MicroRNA-195 targets ADP-ribosylation factor-like protein 2 to induce apoptosis in human embryonic stem cell-derived neural progenitor cells. *Cell Death Dis* **4**, e695
60. Ohba, S., Kamata, K., and Miki-Noumura, T. (1993) Stabilization of microtubules by dynein-binding in vitro. Stability of microtubule-dynein complex. *Biochim Biophys Acta* **1158**, 323-332
61. Piontek, K., Menezes, L. F., Garcia-Gonzalez, M. A., Huso, D. L., and Germino, G. G. (2007) A critical developmental switch defines the kinetics of kidney cyst formation after loss of Pkd1. *Nat Med* **13**, 1490-1495